Project 4 - The orbit of BH and NS

Nicolò Belgiovine, Martina Cacciola, and Konstantinos Panagiotakis
(Dated: March 26, 2024)

This project focuses on the evolution of massive stars ($> 10M_\odot$) ending in supernova (SN) explosions, resulting in black holes (BH) or neutron stars (NS). The study investigates how asymmetries in mass ejection during explosions affect the orbits of BH and NS remnants in the Milky Way (MW). Exploiting N-body simulations, we integrate high-mass stars in disc-like orbits, incorporating velocity kicks upon explosion. The analysis explores spatial properties of the remnant population based on kick models, remnant type, and metallicity. Using SEVNpy for stellar evolution and kicks, the simulations provide insights into the effects of different parameters on the distribution of compact remnants.

INTRODUCTION

Numerical N-body simulations involve the computation of forces acting on N particles over a time period t. These simulations are particularly important in astrophysics as they model the evolution of celestial structures, which are governed by the dynamical interactions between bodies under gravitational forces. This approach helps to understand large-scale structure problems (e.g. the formation and evolution of galaxies) and to investigate the dynamics of star clusters. Potential estimates are crucial: they provide a measure of the gravitational potential at each point in space, used then for calculating the forces experienced by each particle. An interesting application is the study of the spatial distribution of the remnants of high-mass stars. When massive stars ($> 10M_\odot$) die via core-collapse SN explosion, they leave behind a compact object (either a NS or a BH), expected to receive a spatial velocity at its birth because of asymmetric mass ejection. For NSs, we can reconstruct the distribution of kick magnitudes from observations of proper motions of Galactic pulsars, thanks to the radio jet powered by high-velocity rotation and magnetic field. Instead, for BHs the data are scanty and complex to interpret, as their detections come from indirect methods, e.g. gravitational micro-lensing or the observation of BH-star systems. Thus, the constraints on the kick distribution represent still an open question.

METHODS

In this project, we will leverage N-body simulations to integrate massive stars in disc-like orbits until explosion. At this point, the compact object is subject to both its orbital velocity and the velocity kick. The remnant will then be studied in its evolution for $3-5$ Gyr: the aim is to investigate the spatial properties of the population of NSs and BHs, depending on the remnant type, the kick model and the metallicity.

Code packages

To initialize and evolve a N-body simulation, we use **Fireworks** ([1]), a Python package with a series of tools for collisional/collisionless systems and orbit integration. It contains wrappers to other integrators such as **Pyfalcon** ([2]) and **TSUNAMI** ([3]). It takes as input an instance of the class `Particles` with specified initial conditions and a function to estimate the acceleration from the module `dynamics` (or `potentials`). Then, we iteratively integrate until reaching the required evolution time. To insert additional physics, we can couple the simulations with the population synthesis code **SEVN** (Stellar EVolution N-body) ([4], [5]). It includes stellar evolution via interpolation of precomputed stellar tracks (from PARSEC and MIST), binary evolution, and different recipes for core-collapse supernovae. In such a way, while updating the dynamics, we are evolving also the stellar properties in a reasonable amount of computational time. We have to keep in mind that once we include additional physics, the N-body simulations are not scale-free anymore: the N-body units from Fireworks must be converted into physical units for SEVN, and vice-versa. In our case, we set the proper scaling for the MW by setting the N-body units to: $M_{\rm scale} = 10^{10}\,M_\odot$, $r_{\rm scale} = 1000\,{\rm pc} = 1\,{\rm kpc}$, and $T_{\rm scale} = 1000\,{\rm Myr} = 1\,{\rm Gyr}$.

Astrophysical tools

Potential

For the **MW potential**, we use the Johnston's model ([6]). It includes a Hernquist potential for the inner spheroid, assuming spherical symmetry:

$$\Phi_{\rm spher}(r) = -\frac{GM_{*,spher}}{r+c} \tag{1}$$

where $c = 0.7\,{\rm kpc}$ (scale length parameter) and $M_{*,spher} = 3.4\times10^{10}\,M_\odot$. Then, it considers a Myamoto-

Nagai disk:

$$\Phi_{\rm disk}(R,z) = -\frac{GM_{*,disc}}{\sqrt{R^2 + \left(a + \sqrt{z^2+b^2}\right)^2}} \tag{2}$$

where the scale length parameters are $a = 6.5\,\mathrm{kpc}$, $b = 0.26\,\mathrm{kpc}$ and $M_{*,disc} = 10^{11} M_\odot$. Finally, for the Dark Matter halo, it involves a logarithmic potential:

$$\Phi_{\rm halo}(r) = v_{halo}^2 \ln(r^2 + d^2) \tag{3}$$

where $v_{\rm halo} = 212\,\mathrm{km\,s^{-1}}$ is the circular velocity at large radius and $d = 12\,\mathrm{kpc}$ is the core radius.

Initialization

To generate a disc-like stellar population, we need to define the initial conditions of the N-body problem. We are considering the stars as tracer particles of the potential, hence not intended to produce gravitational potential themselves (which will be anyway much weaker than the overall MW potential). If we are interested in simulating a stellar population of the Galactic disk, we can assume stars to be in nearly circular orbits in a disk-like distribution. The initial phase-space **positions** are drawn from a double-exponential profile describing the mass distribution ([7]):

$$\rho(R,z) = \frac{M_{disk}}{4\pi R_d^2 z_d} e^{-R/R_d} e^{-|z|/z_d} \tag{4}$$

where M_{disk} is the total mass of the disk, R_d is the length scale ($= 2.6\,\mathrm{kpc}$ for a thin-disk like population) and z_d the height scale ($= 0.3\,\mathrm{kpc}$). The disk probability density function is $f(R,z) = \rho(R,z)/M_{disk}$. The density profile can be split into two parts, by separating the two dependencies: $f(R,z) = g(R)h(z)$. With some manipulations, we can obtain:

$$G(R) = 1 - e^{-x}(1+x) = u_R \tag{5}$$

$$H(z) = 1 - e^{-|z|/z_d} = u_z \tag{6}$$

where in Eq.5 $x = R/R_d$. Thus, R and z can be sampled from $u_R \sim \mathcal{U}(0,1)$ and $u_z \sim \mathcal{U}(0,1)$ interpolating the cumulative density function (cdf) and using the inverse sampling. We start with a non-invertible cdf $F(x)$ by assuming the range $[x_{min}, x_{max}]$ from which x should be drawn. The cdf is evaluated in a grid of x values, then these results are subject to scaling to ensure $F(x_{min}) = 0$ and $F(x_{max}) = 1$. At this point, we perform the interpolation by using as input values sampled from $\mathcal{U} = (0,1)$. The sign of z can be obtained by randomly drawing a third random uniform number u and assigning the positive sign if $u < 0.5$, the negative sign otherwise. The azimuthal angle can be drawn from a uniform distribution, $\Phi \sim \mathcal{U}(0, 2\pi)$. This can be done using $X = u(x_{min} - x_{max}) + x_{min}$, where X follows $\mathcal{U}(x_{min}, x_{max})$.

The initial **velocities** can be sampled from the cylindrical space $\vec{v} = (v_R, v_\Phi, v_z)$ and then converted into Cartesian, as follows:

$$\begin{bmatrix} v_R \\ v_\phi \\ v_z \end{bmatrix} = R^T(i,\phi) \begin{bmatrix} v_x \\ v_y \\ v_z \end{bmatrix}$$

where

$$R(\phi) = \begin{bmatrix} \cos\phi & -\sin\phi & 0 \\ \sin\phi & \cos\phi & 0 \\ 0 & 0 & 1 \end{bmatrix}$$

The particles are assumed to have an azimuthal circular velocity: $v_{circular} = \sqrt{R a_R}$. Here a_R represents the total acceleration in the radial direction due to the external potential, evaluated at point (R,z) using the MW potential. In cylindrical coordinates, we can extract the velocity distribution for its three components from Gaussians:

$$\begin{aligned} v_R &\sim \mathcal{N}(0, \sigma_R) \\ v_\Phi &\sim \mathcal{N}(v_{\rm circ}, \sigma_\Phi) \\ v_z &\sim \mathcal{N}(0, \sigma_z) \end{aligned}$$

where σ_R, σ_Φ and σ_z are the velocity dispersion. In case of a thin-disk population, they assume the values: $\sigma_R = 36$ km/s, $\sigma_\Phi = 24$ km/s and $\sigma_z = 16$ km/s ([8]). To implement this procedure, we start by assuming the parameters R_d and z_d for the spatial distribution, the external potential generating the total radial acceleration a_R and the standard deviations σ_R, σ_Φ, σ_z. The steps are repeated for the drawn phase-space positions of every particle.

The initial **masses** are drawn using a Kroupa initial mass function (IMF) [9], from $M_{\rm min} = 9\,M_\odot$ to $M_{\rm max} = 150\,M_\odot$. We are not considering masses below $9\,M_\odot$, since we are only interested in compact remnants (hence, we exclude white dwarfs with $M < 8 - 9\,M_\odot$). The IMF describes the probability of a star having a certain mass during its formation. In particular, the Kroupa IMF is a piecewise power-law function that describes the distribution of stellar masses in young star clusters:

$$f(x) = \begin{cases} K_1 x^{-0.3}, & \text{if } x \le 0.08 \\ K_2 x^{-1.3}, & \text{if } 0.08 < x \le 0.5 \\ K_3 x^{-2.35}, & \text{if } x > 0.5 \end{cases}$$

where $x = \frac{m^*}{M_0}$ and K_1, K_2, K_3 are normalization constants for the different segments of the piecewise power-law function. In our case, we only use the third equation of the system and compute K as follows:

$$K = \frac{1}{\ln M_{\rm max} - \ln M_{\rm min}}$$

To draw the values for the initial masses, we generate a random number and then use the inverse of the cumulative distribution function (CDF) of the IMF to get the corresponding stellar mass.

Stellar evolution

We start by initializing particles using the positions, masses and velocities sampled before. A list of stars for each of the bodies in the simulation is evolved over a certain time, until the formation of a compact remnant. Particles go inside an integration loop using **Verlet integrator**:

$$\begin{aligned} \mathbf{r}_{i+1} &= \mathbf{r}_i + \mathbf{v}_i h + \tfrac{1}{2}\mathbf{a}_i h^2 \\ \mathbf{a}_{i+1} &= f(\mathbf{r}_{i+1}) \\ \mathbf{v}_{i+1} &= \mathbf{v}_i + \tfrac{(\mathbf{a}_i + \mathbf{a}_{i+1})}{2} h \end{aligned}$$

in which the acceleration does not depend on the velocity. The position and velocity are synchronized, resulting useful to analyse N-body outputs. The integration is divided into three specific periods: the evaluation happens at the beginning of the evolution, before any kick occurs, at the SN explosion when the kick takes part and after it. During the explosion, the velocity kick (with components on x, y and z) is added to the current velocity of the object. Then, the total energy acquired is computed: in case of a positive value, the particle is expelled by the system, meaning it is not gravitationally bound anymore.

Natal kicks

The spatial velocity received by the compact remnant at its birth has to be addressed to asymmetries in the mass ejection and/or in the neutrino emission, during core collapse ([10]). The knowledge about NSs is definitely wider. Based on observational estimates of pulsar proper motions, Hobbs et al. ([11]) proposed a 3D velocity distribution of pulsars, from observations of 2D distribution of pulsars. It consists of a Maxwellian distribution with root-mean-square velocity $\sigma = 265$ km/s. Another proposal is a bimodal velocity distribution ([12] and [13]) with a first peak at low velocities and a second one at high velocities. Although the engine leading to the formation of the compact object is roughly the same, the study concerning BHs is filled with uncertainties. In the treatment of BHs, it is important first to establish if the BH comes from fallback or direct collapse. The former case gives birth to lighter BHs, whose natal kicks resemble the same distribution as NS kicks but are corrected either for linear momentum conservation ([14]:

$$v_{\rm kick,BH} = \frac{m_{\rm NS}}{m_{\rm BH}} v_{\rm kick,NS} \tag{7}$$

or the effect of fallback ([15]):

$$v_{\rm kick,BH} = (1 - f_{\rm fb}) v_{\rm kick,NS} \tag{8}$$

where $f_{\rm fb}$ is the fall-back parameter. The latter produces massive BHs, resulting extremely gravitationally bound and thus no kick is usually assumed apart from *Blaauw kick* ([16]). If the SN occurs in a binary star, even if the mass loss is completely symmetric, a non-negligible kick is expected to affect the orbital properties of the binary system. It has to be attributed solely to the rapid mass loss succeeding the SN explosion. If the binary remains bound, it means that the mass loss must be $< 0.5(M_{\rm He} + m)$, where $M_{\rm He}$ is the mass of the progenitor helium star and m is the mass of the donor star. Other prescriptions take into account both the momentum conservation and the asymmetries using the ejecta mass $m_{\rm ej}$ (e.g. [17], [18]):

$$v_{\rm kick,rem} \propto m_{\rm rem}^{-1} m_{\rm ej} \tag{9}$$

where $m_{\rm rem}$ is the mass of the remnant.

RESULTS

In our work, we focus on two models of velocity kicks, the pure Hobbs model with $\sigma = 265$ km/s and a Hoobs model in which the kicks are **rescaled** by the fraction of material that falls back on the proto-remnant during the SN explosion ($\sigma = 150$ km/s, which can be attributed to [19]). This second prescription assumes that the BHs receive lower kicks with respect to NSs. We evolve 1000 stars (a sufficient number to get a good insight into the statistical properties) over a period of 3 Gyr, using a timestep of 0.01 Gyr. We explore two different metallicities: $Z = 0.002$ corresponding to an older and metal-poor population, and $Z = 0.002$ typical of a young metal-rich disk population. Our goal is to show the **spatial distribution** of the particles during their evolution, tracking the stars until they end their life into a BH or a NS. As the outer layers of the star are expelled in the SN, the remaining compact core experiences a recoil effect, propelling it away from the center of the explosion. In Fig.1, we can see the motion in the x-y plane of the stars we have initialized in the simulation. The results are in line with our assumptions, since we have put stars in a nearly circular orbit and we are considering them as tracer particles, not creating their gravitational potential. They will continue to follow their paths around the Galactic center under the influence of the MW potential. Stars within the system will undergo their evolution, with more massive stars evolving faster. This can lead to the ejection of mass through stellar winds or SN explosions, affecting the overall dynamics of the system. The magnitude of the kick velocity depends on various factors, and it can range from a few hundred to several thousand kilometers

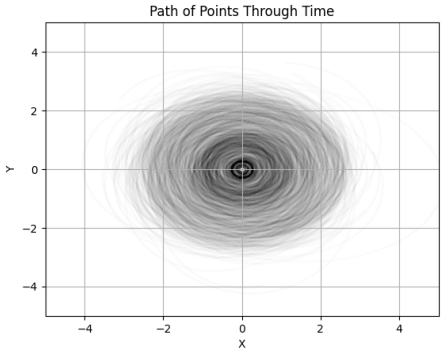

FIG. 1. Orbital motion of the simulated stars over a period of 3 Gyr, using Hobbs model with $\sigma = 265$ km/s and a metallicity $Z = 0.002$.

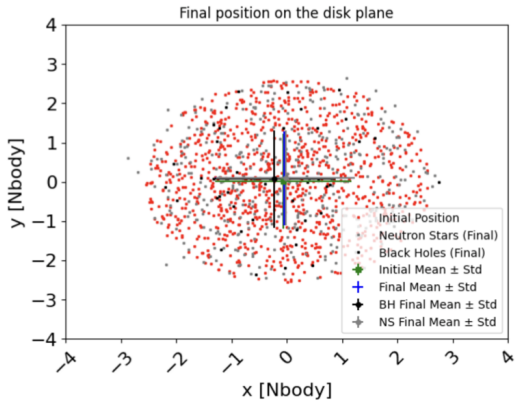

FIG. 2. Position on the x-y plane of the stars in the simulation (in red), which end up in the NSs (in gray) and in the BHs (in black). The average initial and final position with the relative standard deviations are also depicted. The model used is pure Hobbs with $\sigma = 150$ km/s and $Z = 0.002$.

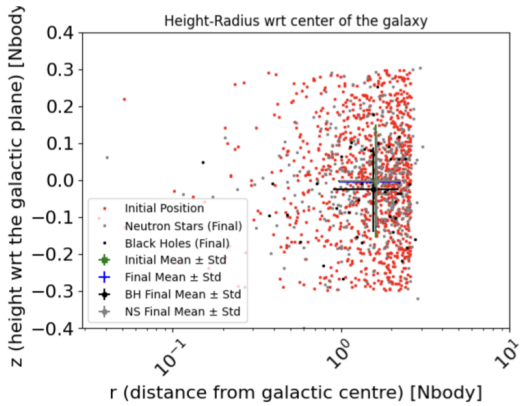

FIG. 3. Radius r (distance from the galaxy center) versus height z computed with respect to the galactic plane. The model used is pure Hobbs with $\sigma = 150$ km/s and $Z = 0.002$.

per second. NSs and BHs propelled by these kicks can travel significant distances from their birthplaces in the host galaxy. The actual distance traveled by these compact remnants is determined by the strength of the kick, the mass of the remnant, and the density of the surrounding interstellar medium. In some cases, these objects can be ejected from their original galaxies and become part of the intergalactic medium.

In Fig.3, we show the x-y position of particles with respect to the disk plane of the MW. Initially, the stars in the system are uniformly distributed across a more or less spherical surface. Compared to BHs, NSs tend to be more numerous: due to the lower masses, they respond more sensitively to external forces. This results in a higher probability of traveling larger distances at parity of the kick received, thus reflecting a more widespread dispersion in the disk plane. It has been proved that a large fraction of NSs is able to leave the MW in the case of the high velocities reached being of the same order of the escape velocity from the Galaxy ([20]). On the other hand, because of their increased gravitational influence, BHs tend to depart less from the central regions of the stellar system. BHs may also form through direct collapse without a SN explosion, leading to a lack of a significant kick. Without a strong kick, BHs are less likely to gain high velocities that would carry them far from their formation region. A more in-depth study of their locations can be found in [21].

In Fig.3 we show the position of the particles calculated over the galactic plane, in case of a thin disk population. NSs exhibit a distribution that reflects their formation history and subsequent dynamical evolution. We can see a range of heights above the galactic plane, with some neutron stars dispersed throughout the disk and others concentrated toward specific heights. BHs, especially more massive ones, might show a concentration toward the central regions of the galaxy. This concentration can be a result of dynamical processes, such as gravitational interactions and mass segregation, causing BHs to sink toward the galactic center over time.

We decided also to analyze the distribution of some interesting features, using smoothed Kernel Density Estimation (KDE) curves. We started with the **mass distribution** of the compact remnants for each of the two models, showing what happens at different metallicities. The trend for the **BH** masses from pure Hobbs model in Fig.5 is explained by addressing the relation between mass loss and metallicity: $\dot{m} \propto Z^{0.85}$. BHs can be formed from the collapse of massive stars that have lost their outer layers due to strong stellar winds or binary interactions. The mass of a BH is determined by the mass of the progenitor star's core at the time of collapse, as well as the amount of mass that falls back onto the BH after the supernova. Higher metallicities translate into more electrons in the progenitor star (i.e. more transitions with smaller energy difference). Hence, stronger stellar winds

cause massive stars to lose their outer layers ([22]). This results in lighter objects (in our case, there are two peaks at $\sim 10\,M_\odot$ and $20\,M_\odot$), with respect to the case of lower metallicity (a broader maximum is reached at $\sim 30\,M_\odot$). The mass distribution of NSs remains the same for different metallicities (assessing at $\sim 1.35 M_\odot$, see Fig.5). This value is primarily determined by the mass of the progenitor star's core at the time of the supernova, which is relatively insensitive to the star's metallicity ([23]). Their typical mass is about $1.4 M_\odot$ (known as Chandrasekhar limit). It represents the maximum mass that a star can have and still be supported against gravitational collapse by neutron degeneracy pressure. A similar behaviour for both BHs and NSs is seen for the Hobbs model with $\sigma =$ 265 km/s.

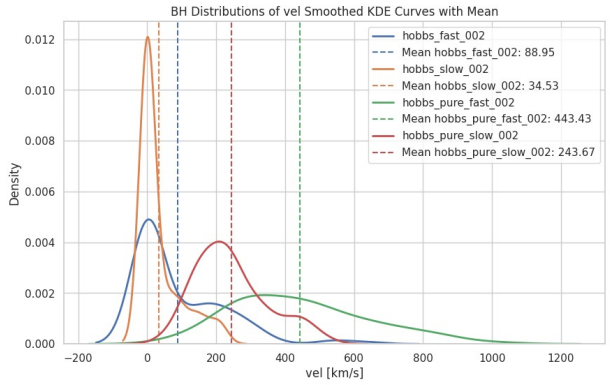

FIG. 4. Distribution of kick velocities of BHs at metallicity $Z = 0.002$. The comparison is done between the models Hobbs and Hobbs pure, considered at $\sigma = 265$ km/s and 150 km/s.

We then studied the magnitude of the **velocity kick** received, focusing on BHs in Fig. 4. We keep the metallicity fixed to analyze the differences between the models. For higher metallicities, the mass loss results in a weaker explosion, which in turn imparts a smaller kick on the remnant. That is because less mass is available to drive the explosion and propel the object away. Vice versa, at lower metallicities, the larger retained mass causes a stronger kick. When considering $\sigma = 265$ km/s, we will have a broader distribution of kick velocities, with a longer tail at large velocities. This means that there is a higher probability for BHs to receive very high or very low kick velocities compared to the model with $\sigma = 150$ km/s. The latter has a narrower distribution, with most BHs receiving a recoil of speed closer to the mean of the distribution. The pure Hobbs model is expected to produce heavier BHs because of the fraction of the fall-back material. These objects will be less prone to be kicked out at high velocities because of the increased gravitational pull (the mean velocity received is between 30-70 $M_\odot$). The pure Hobbs model gives instead higher velocities, with two peaks for the two σ considered respectively at ~ 250 km/s and 400 km/s.

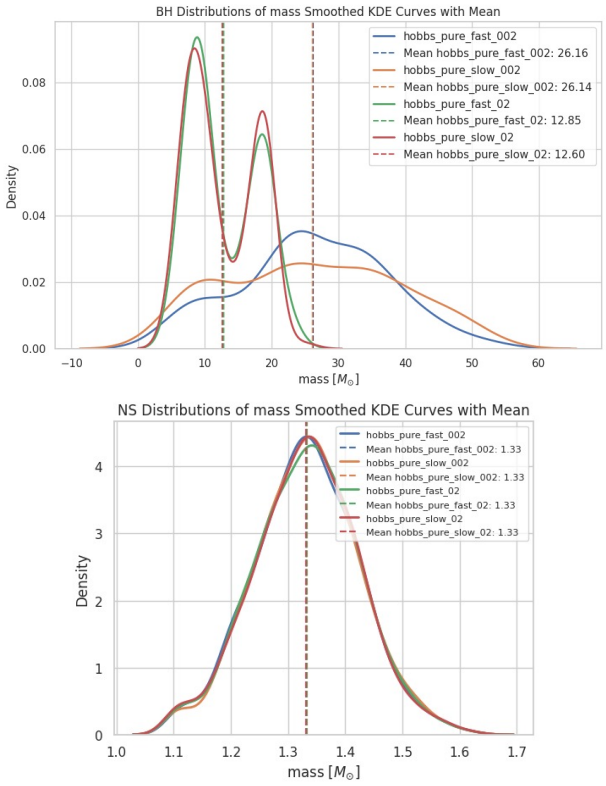

FIG. 5. Distribution of BH and NS masses (respectively top and bottom panel) in case of the pure Hobbs model. The curves correspond to different combinations of the following parameters: σ= 265 km/s, 150 km/s; Z= 0.2, 0.002.

CONCLUSIONS

In our study, we employed N-body simulations to investigate how asymmetries in mass ejection during these explosions influence the orbits and spatial distribution of the resulting remnants in the Milky Way. To do so, we have incorporated various factors such as kick models, remnant types, and metallicities. We observed distinct spatial distributions of NSs and BHs, with NSs exhibiting a more widespread dispersion across the galactic plane compared to BHs, which tend to gravitate toward the central regions of the galaxy. This arises from the differing responses of NSs and BHs to external forces. Furthermore, we explored the mass distributions of NSs and BHs, finding that the mass distribution of BHs is significantly influenced by metallicity, because of the presence of stellar winds. In contrast, the mass distribution of NSs remains relatively consistent across varying metallicities. By integrating N-body simulations with stellar evolution models and astrophysical prescriptions for kick velocities, we offer valuable insights into the complex interplay between stellar dynamics, SN explosions, and the formation of compact remnants in galactic environments.

REFERENCES

[1] G. Iorio, Fireworks documentation, https://ca23-fireworks.readthedocs.io/en/latest/.

[2] PYFALCON documentation, https://github.com/GalacticDynamics-Oxford/pyfalcon.

[3] A. A. Trani, M. Spera, *Proceedings of the International Astronomical Union* **2020**, *16*, 404–409.

[4] G. Iorio et al., SEVN documentation, https://ca23-fireworks.readthedocs.io/en/latest/.

[5] G. Iorio et al., **2023**, *524*, 426–470.

[6] K. V. Johnston et al., *Astrophys. J.* **1995**, *451*, 598.

[7] P. J. McMillan, *Monthly Notices of the Royal Astronomical Society* **2011**, *414*, 2446–2457.

[8] A. C. Robin et al., *Astronomy amp; Astrophysics* **2004**, *416*, 157–157.

[9] P. Kroupa, *Monthly Notices of the Royal Astronomical Society* **2001**, *322*, 231–246.

[10] H.-T. Janka, *Annual Review of Nuclear and Particle Science* **2012**, *62*, 407–451.

[11] G. Hobbs et al., *Monthly Notices of the Royal Astronomical Society* **2005**, *360*, 974–992.

[12] C. Fryer et al., *The Astrophysical Journal* **1998**, *496*, 333–351.

[13] Z. Arzoumanian et al., *The Astrophysical Journal* **2002**, *568*, 289–301.

[14] M. Mapelli et al., *Monthly Notices of the Royal Astronomical Society* **2013**, *429*, 2298–2314.

[15] C. L. Fryer et al., *The Astrophysical Journal* **2012**, *749*, 91.

[16] A. Blaauw, **1961**, *15*, 265.

[17] J. C. Bray, J. J. Eldridge, *Monthly Notices of the Royal Astronomical Society* **2018**, *480*, 5657–5672.

[18] N. Giacobbo, M. Mapelli, *The Astrophysical Journal* **2020**, *891*, 141.

[19] P Atri et al., *Monthly Notices of the Royal Astronomical Society* **2019**, *489*, 3116–3134.

[20] N. Sartore et al., *Astronomy and Astrophysics* **2010**, *510*, A23.

[21] A. Olejak et al., *Astronomy amp; Astrophysics* **2020**, *638*, A94.

[22] A. Romagnolo et al., On the maximum black hole mass at solar metallicity, **2024**.

[23] B. Kiziltan et al., The Neutron Star Mass Distribution, **2010**.